Chapter 3

Effect of calcium (Ca) dopant at 'A' site in tuning the ferroelectricity of average cubic ($Pm\bar{3}m$) phase in a perovskite (ABO_3)-based lead-free ($Ba_{1-x}Ca_x$)($Sn_{0.11}Zr_{0.05}Ti_{0.84}$)$O_3$ system

3.1 Introduction

The scientific and technologically important barium titanate ($BaTiO_3$) based solid solutions such as (Ba,Ca)TiO_3, Ba(Zr,Ti)O_3, Ba(Sn,Ti)O_3, (Ba,Ca)(Zr,Ti)O_3, (Ba,Ca)(Sn,Ti)O_3 and (K,Na,Ba)(Ti,Nb)O_3, etc. has proven itself, as a potential replacement of toxic and hazardous lead-based materials [8, 11, 13, 34, 44, 46, 225]. These solid solutions find wide applications in high-density energy storage devices, transducers, multilayer ceramic capacitors, infrared detectors, microwave dielectric amplifiers, phase shifters, memory

devices, etc. [43, 44, 164, 179]. The parent compound $BaTiO_3$ possesses three different temperature-driven polarization states, *viz.,* $\langle 111 \rangle$, $\langle 110 \rangle$, $\langle 100 \rangle$, corresponding to their respective ferroelectric rhombohedral (R; *R*3*m*), orthorhombic (O; *Amm*2) and tetragonal (T; *P*4*mm*) phases, and finally attains a paraelectric cubic (C; $Pm\bar{3}m$) phase at high temperature. All the phases of $BaTiO_3$ exhibit locally off-centered B(Ti^{4+}) site cation along $\langle 111 \rangle$ direction, compatible with the constraints of its low-temperature rhombohedral phase [182, 183, 231]. The ferroelectric and piezoelectric properties of barium titanate can be tuned via temperature, pressure, particle size, dimension, or by substitution at A (common dopants: Sr^{2+}/Ca^{2+}) or (and) B (common dopants: Zr^{4+}/Sn^{4+}) sites. On substituting, Zr^{4+}/Sn^{4+} at the 'B' site, the phase transitions corresponding to $BaTiO_3$ approach each other and eventually coalesce slightly above room temperature for $\sim$ 15 mol% of Zr and $\sim$ 11 mol% of Sn respectively, where significantly enhanced dielectric and ferroelectric properties have been observed [8, 46, 180, 187, 189]. Moreover, the solid solution $Ba(Zr,Ti)O_3$ undergoes a conventional ferroelectric to diffuse ferroelectric phase transition for $\sim$ 15 mol% of Zr. On further increasing Zr content, it exhibits a relaxor ferroelectric nature for $\sim$ (25-75) mol%, after that shows a dipolar glass-like behaviour up to $\sim$ 95 mol% of Zr, and finally a weak incipient ferroelectric nature for end member $BaZrO_3$ [46, 176, 180, 189]. A similar phase transition behaviour, with normal ferroelectric to relaxor crossover beyond $\sim$ 20 mol% of Sn in $Ba(Sn,Ti)O_3$ has been observed [9, 47, 166, 168, 232]. Similarly, A(Ca^{2+})-site driven polarization in $(Ba,Ca)TiO_3$ enhances the dielectric and ferroelectric properties of $BaTiO_3$. Incorporation of Ca^{2+} sustains the Curie temperature while decreases the inter-ferroelectric phase transition temperatures [44, 160, 233]. Earlier, Fu *et al.* reported an off-centering tendency of Ca^{2+} cation in $(Ba,Ca)TiO_3$ along [113] direction, owing to its smaller size than Ba^{2+} cation, and observed a cooperative behaviour of the dipoles corresponding to 'A' and 'B' sites [7, 49]. The effect of simultaneous doping on 'A' and 'B' sites of $BaTiO_3$ has also been studied by various groups. Liu and Ren reported a

huge piezoelectric coefficient $d_{33} \sim 620$ pC/N for $Ba(Ti_{0.80}Zr_{0.20})O_3$-$x(Ba_{0.70}Ca_{0.30})O_3$ system at the morphotropic phase boundary (MPB) and attributed this high piezoresponse to the low energy barrier between the coexisting macroscopic $\langle 100 \rangle$ (tetragonal) and $\langle 111 \rangle$ (rhombohedral) polarization states. This low energy barrier facilitates easy polarization rotation between the two polarization states, *viz.,* $\langle 100 \rangle$ and $\langle 111 \rangle$ [11, 115]. However, recent studies have shown two types of phase boundaries, *viz.,* T-O and O-R, rather than a single T-R phase boundary, with the highest piezoresponse at the T-O phase boundary, and attributed this to the lower energy barrier between the T-O phases in comparison to O-R phases [12, 201]. Recently, in relaxor ferroelectric system (K,Na,Ba)(Ti,Nb)O_3 (exhibiting an average cubic symmetry), a similar polarization rotation (as observed by Liu and Ren in $Ba(Ti_{0.80}Zr_{0.20})O_3$-$x(Ba_{0.70}Ca_{0.30})O_3$ ceramics [11]), between coexisting microscopic $\langle 100 \rangle$ and $\langle 111 \rangle$ polarization states at morphotropic relaxor boundary (reminiscent of the MPB of normal ferroelectrics) has been observed [225]. The existence of morphotropic relaxor boundary (MRB) was found to increase the dielectric permittivity, and the electrostrain over a wide temperature range [225]. Some groups have reported high ferroelectric and piezoelectric properties in another $BaTiO_3$-based ceramic system (Ba,Ca)(Sn,Ti)O_3 [13, 43, 45, 202]. Therefore it is of great interest to study the A(Ca^{2+}) and B(Sn^{4+}/Zr^{4+})-site doped $BaTiO_3$-based solid solutions. Owing to the above analysis, we have fabricated the solid solution $(Ba_{1-x}Ca_x)(Sn_{0.11}Zr_{0.05}Ti_{0.84})O_3$; BCSZT$x$ ($0 \leq x \leq 0.20$) for complete structural investigation and its relation with various ferroelectric properties. The presence of Ca^{2+} at the 'A' site is expected to be off-centered relative to Ba^{2+} due to its relatively smaller ionic radii. Also, the proposed system may exhibit the relaxor behaviour because of the difference in ionic radii and ferroelectric strength of the cations corresponding to the 'A' and 'B' sites.

3.2 Experimental procedure

All the BCSZTx; $0 \leq x \leq 0.20$ ceramics were synthesized via a conventional solid-state reaction method. The raw materials $BaCO_3$, $CaCO_3$, TiO_2, SnO_2, and, ZrO_2 were weighed in stoichiometric amounts, and ball milled for 24 hours in acetone as milling media. Then ball milled powders were dried and calcined at 1100 ^{0}C for 6 hours. Thereafter, calcined powders were crushed and mixed with 2% PVA binder and pelletized at 6 metric tons pressure. The green pellets thus formed were sintered at 1350 ^{0}C for 12 hours. The relative density of sintered pellets was found to be more than 97%. The sintered pellets were again crushed and annealed at 300 ^{0}C for 4 hours. The X-ray powder diffraction data of the annealed powders were collected within the 2θ range 20^0-120^0 with a step interval of 0.02^0, using Rigaku Smart Lab high-resolution X-ray diffractometer having Cu-$K_{\alpha 1}$(λ = 1.54059 Å) radiation. For dielectric measurements, we deposited the silver electrodes on both sides of the sintered pellets and performed the temperature-dependent dielectric measurement at several different frequencies between 100 Hz-1 MHz using HP4194A impedance analyser. The PE loop measurement was conducted at Radiant Technology's Precision Material Analyzer Workstation based on the virtual ground system at 50 Hz frequency. The room temperature Raman spectroscopic measurements have been carried out over the wavenumber range 50-1000 cm^{-1} using Renishaw InVia Raman spectrometer (Wotton-under-Edge, UK) at an excitation wavelength of 532 nm.

3.3 Results and discussions

3.3.1 X-ray diffraction studies

The observed X-ray diffraction patterns have shown the formation of solid solution for composition range $0 \leq x \leq 0.15$, except a minor impurity phase of ZrO_2 having a fraction $<1\%$. Moreover, for higher composition, *i.e.,* x = 0.20, an additional calcium titanate like

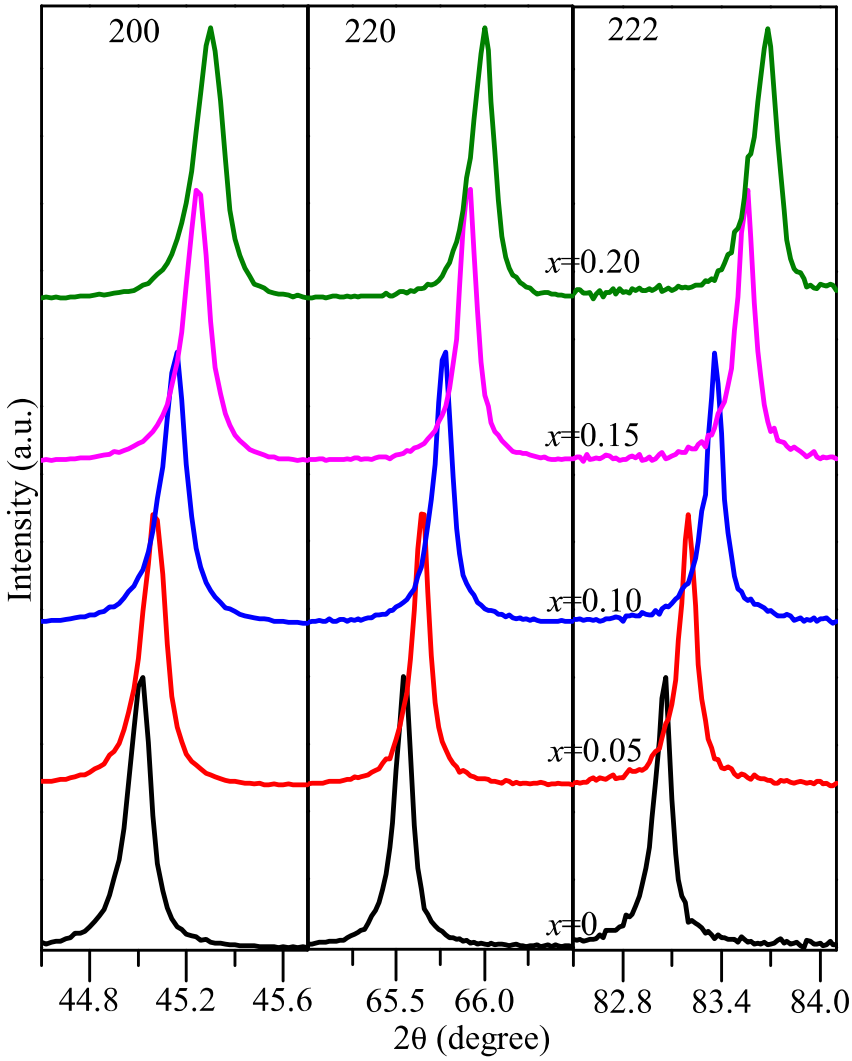

Fig. 3.1 Evolution of 200, 220, and 222, X-ray diffraction peaks for BCSZTx ($0 \leq x \leq 0.20$) ceramics.

phase (shown by an arrow mark in Fig. 3.2(e)) starts appearing. The presence of such a phase in Ca^{2+} doped $BaTiO_3$ is very common and has been previously reported [159, 160, 234]. Further, we observed the non-split nature of the peaks (see Fig. 3.1), which indicates the presence of a cubic phase for all the compositions. To fix the crystallographic structure, we performed the Rietveld refinement of the X-ray diffraction data for all the compositions using the $Pm\bar{3}m$ space group via FULLPROF software [213].

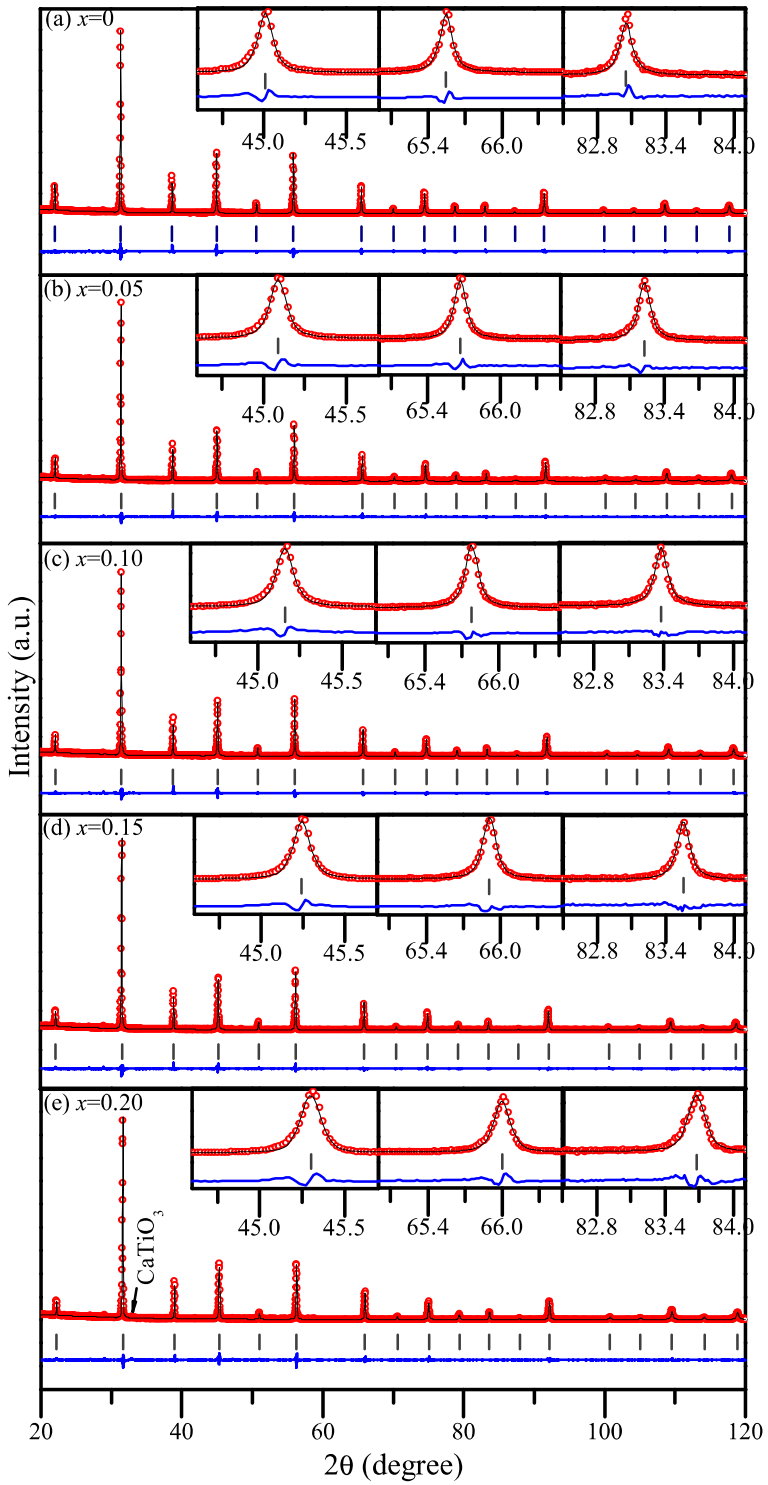

Fig. 3.2 Rietveld refinement plots for X-ray diffraction pattern of BCSZTx ($0 \leq x \leq 0.20$) ceramics using $Pm\bar{3}m$ space group. The observed pattern is represented by open (red) circles, the continuous line (black) represents the simulated patterns, the vertical bars (gray) correspond to Bragg positions, and the continuous lines (blue) below the vertical bars correspond to the difference between observed and simulated patterns.

Table 3.1 Lattice parameters and various agreement factors obtained from Rietveld refinements of room temperature X-ray diffraction data of BCSZTx ($0 \leq x \leq 0.20$) ceramics for cubic ($Pm\bar{3}m$) phase.

x	a (Å)	V(Å^3)	χ^2	R_{wp}	R_{exp}
0	4.02489(2)	65.202(0)	2.31	11.2	7.35
0.05	4.01807(4)	64.871(1)	2.04	10.7	7.50
0.10	4.01210(2)	64.582(1)	2.38	10.8	7.01
0.15	4.00506(2)	64.243(0)	2.28	10.5	6.97
0.20	4.00031(2)	64.015(1)	2.63	11.5	7.06

During refinements, the peak profile was modeled with the pseudo-Voigt function. The background was fitted with a linear interpolation between a set background points with refinable heights. To obtain the best fit between the observed and simulated diffraction patterns, we have refined the parameters like lattice parameters, FWHM parameters, shape parameters, thermal parameters, etc. For BCSZTx ceramics, corresponding to the $Pm\bar{3}m$ space group, Ba^{2+}/Ca^{2+} cations occupy the 1b site with positional coordinate ($\frac{1}{2}, \frac{1}{2}, \frac{1}{2}$), Ti^{4+}/Sn^{4+}/Zr^{4+} occupies the 1a site with position coordinates (0,0,0) and O^{2-} occupies the 3d site with positional coordinates ($\frac{1}{2}$,0,0) respectively. The refinements provide satisfactory fits with the reasonable values of agreement factors (see Fig. 3.2 and Table 3.1). The finally refined values of lattice parameters, unit cell volume, and various agreement factors are given in Table 3.1.

3.3.2 Dielectric studies

The frequency-dependent dielectric measurements performed over a wide range of temperature exhibits only one peak for all the compositions, which corresponds to the merger of all the three-phase transitions, as reported earlier in Ba(Zr,Ti)O_3, Ba(Sn,Ti)O_3, and Ba(Sn,Zr,Ti)O_3 systems [8, 180, 235]. We have observed a diffuse phase transition around the temperature corresponding to the dielectric maxima (T_m) and a shift in T_m towards

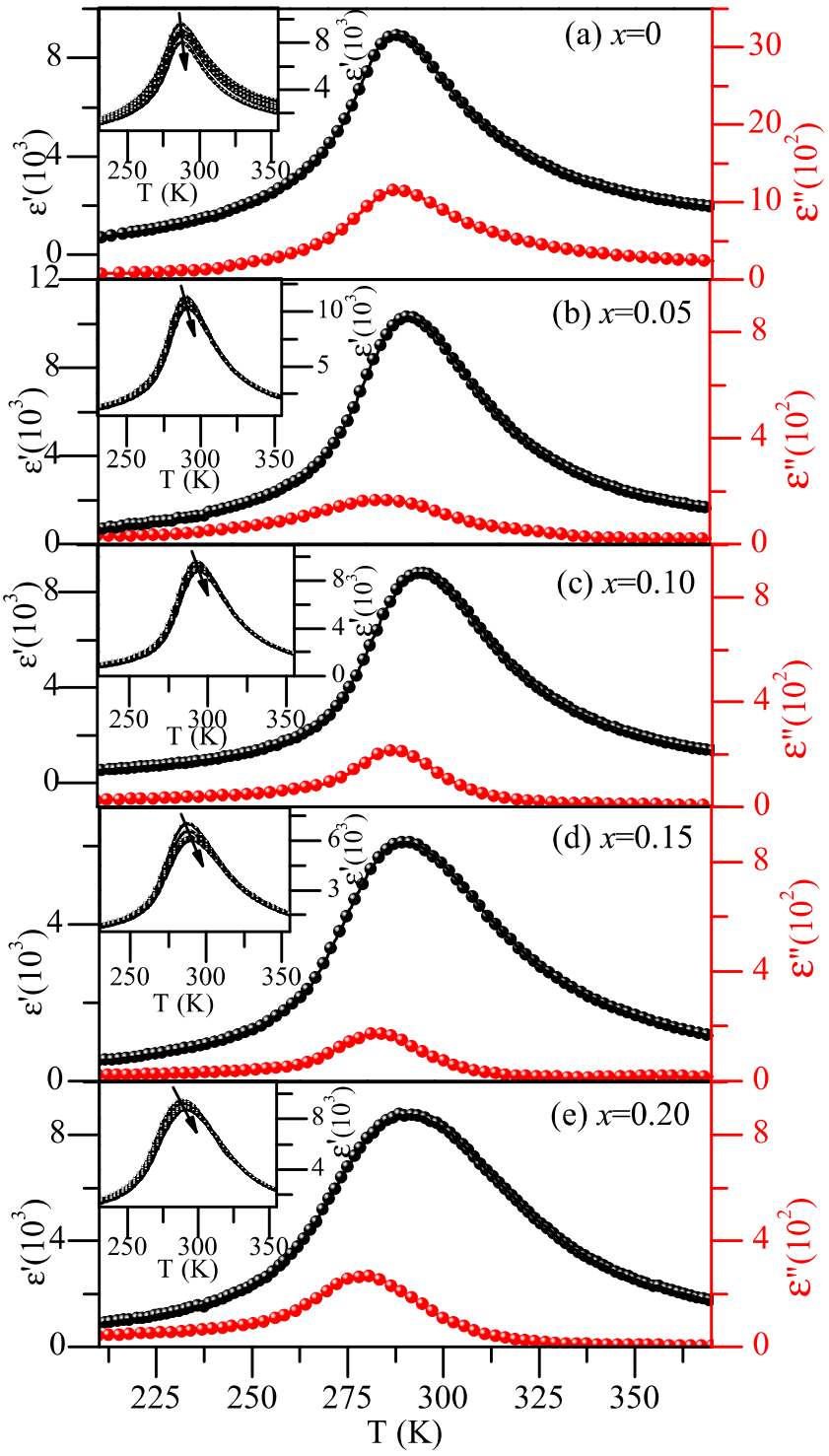

Fig. 3.3 Temperature-dependent variation of real (ε') and imaginary (ε'') parts of dielectric constant for BCSZTx ($0 \leq x \leq 0.20$) ceramics at 100 kHz.

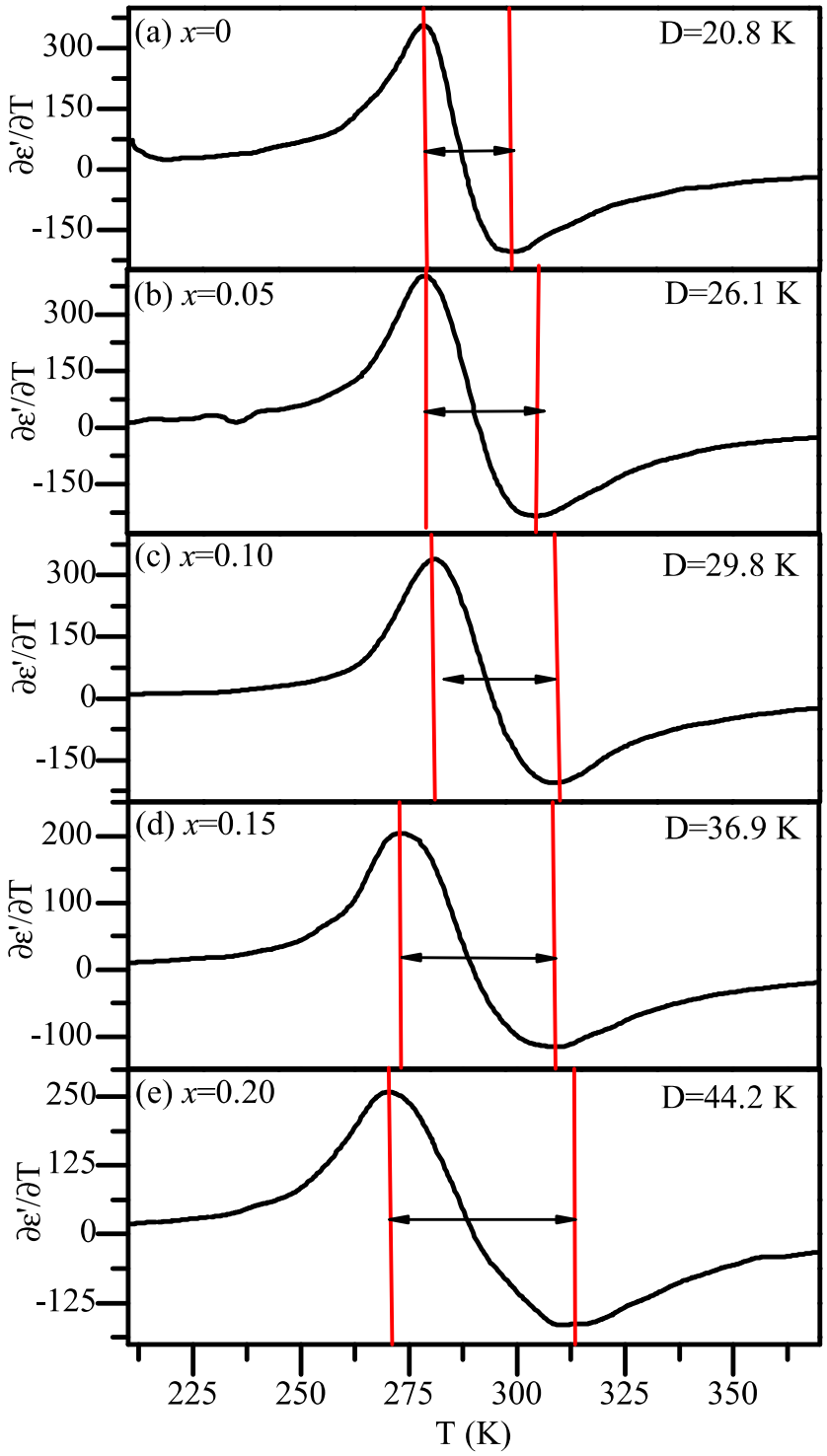

Fig. 3.4 Variation of $\frac{\partial \varepsilon^{'}(T)}{\partial T}$ for BCSZTx ($0 \leq x \leq 0.20$) ceramics at 100 kHz.

the higher temperatures with an increase in frequency, indicating the presence of relaxor ferroelectric nature for BCSZTx ceramics (see inset in Fig. 3.3). Also, the temperature corresponding to the real ($\varepsilon^{'}$) and imaginary ($\varepsilon^{''}$) part of dielectric maxima lie at different temperatures and follow the characteristic feature of relaxors, *i.e.,* T_m ($\varepsilon^{'}$)>T_m($\varepsilon^{''}$) (see Fig. 3.3) [39]. The diffuseness degree characterizing parameter 'D' is defined as [236],

$$D = T_{(\frac{\partial \varepsilon'(T)}{\partial T} min)} - T_{(\frac{\partial \varepsilon'(T)}{\partial T} max)} \tag{3.1}$$

where $T_{(\frac{\partial \varepsilon'(T)}{\partial T} min)}$ and $T_{(\frac{\partial \varepsilon'(T)}{\partial T} max)}$ are the temperatures corresponding to the minimum and maximum value of $\frac{\partial \varepsilon^{'}(T)}{\partial T}$, respectively. The D values show an increasing trend with the increase of x (see Fig. 3.4), indicating that the phase transition becomes more and more diffuse with the increase in $Ca^{2+}(x)$ content. The obtained values of D for x = 0.15 and x = 0.20 are approximately the same as reported earlier in some of the $Ba(Zr,Ti)O_3$ ceramics [236].

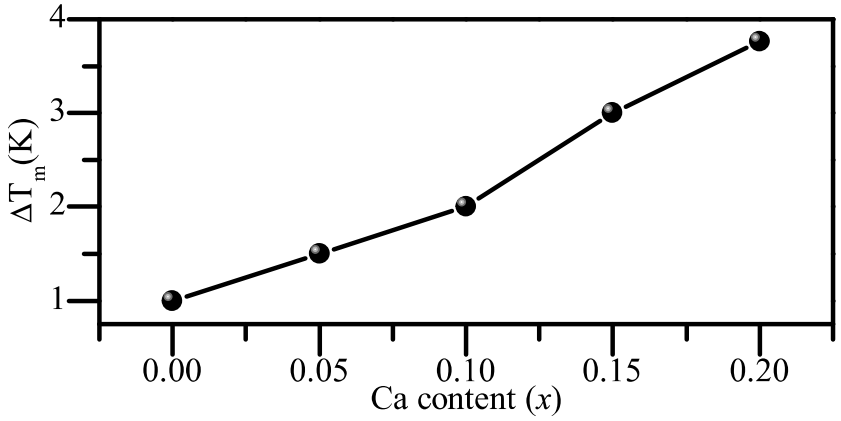

Fig. 3.5 Variation in Δ T_m of BCSZTx ($0 \leq x \leq 0.20$) ceramics.

To further confirm the increase in dielectric relaxor behaviour with the increase in $Ca^{2+}(x)$ content, we have plotted the shift in T_m ($\varepsilon^{'}$) for the change in measurement frequency from 100 Hz to 1 MHz (see Fig. 3.5). The resulting shift (ΔT_m) is, although small, but has an increasing trend with an increase in $Ca^{2+}(x)$ content in BCSZTx matrix. A

similar order of shift ($\Delta T_m < 1\ ^0C$) and the relaxor behaviour over nearly the same frequency range as of BCSZTx has been recently reported in a widely studied (Ba,Ca)(Zr,Ti)O_3 ceramic system [193].

In BCSZTx ceramics, the presence of relaxor behaviour is attributed to the difference in ionic radii and ferroelectric strength of the cations corresponding to 'A' and 'B' sites, respectively. In conventional ferroelectrics such as $BaTiO_3$, a long-range interaction between the dipoles exists. However, within the unit cells in BCSZTx, where ferroelectrically active Ti^{4+}(61 pm) cation is replaced by non-ferroelectric Sn^{4+}(69 pm) in a considerable amount, the dipole can barely occur, and the long-range dipole-dipole interaction is destroyed due to the appearance of paraelectric $BaSnO_3$ like unit cell, and thus the polar nano-regions (PNRs) around Ti^{4+} ions develops [9, 48, 172]. While in the unit cell where Ti^{4+} (61 pm) ion is replaced by Zr^{4+} (72 pm), within the relaxor phase field regime, the PNRs arise due to the presence of random elastic fields. These random fields are generated because of the large difference in ionic radii of Zr^{4+} and Ti^{4+} cations. The replacement of Ti^{4+} by Zr^{4+} cations results in stress at the Ti^{4+} centered octahedra, leading to the reorganization of Ti-O covalent bonds. This results in local displacements of Ti^{4+} cations, depending on the distribution of larger [ZrO_6] and relatively smaller [TiO_6] octahedra. As a consequence of this, the local symmetry of Ti^{4+} cation varies from one unit cell to another and gives rise to an overall random distribution of Ti^{4+} cations leading to the formation of local dipoles with non-vanishing polarization [148, 176, 191, 192]. Further, we see that the diffuseness of dielectric permittivity peak increases with an increase in $Ca^{2+}(x)$ content in the BCSZTx matrix [7, 49, 237]. The substitution of Ba^{2+} (161 pm) with Ca^{2+} (134 pm) at 'A' site results in local elastic fields due to the difference in ionic radii, along with the formation of dipoles owing to the off-centering tendency of Ca^{2+} cation [7, 49].

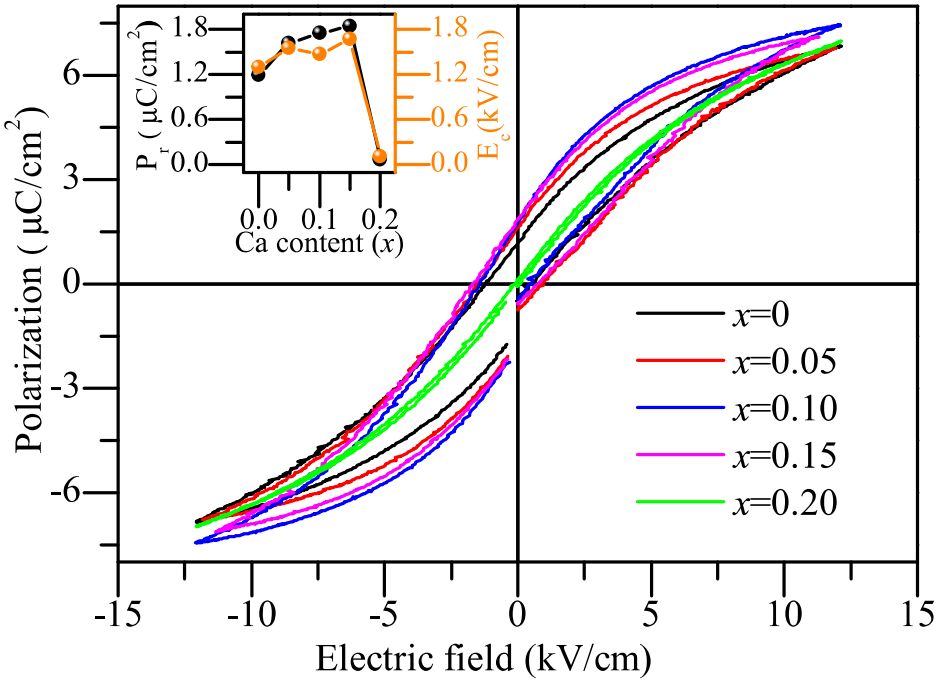

Fig. 3.6 The room temperature PE loop behaviour of BCSZTx ($0 \leq x \leq 0.20$) ceramics.

3.3.3 Polarization *vs.* Electric field (PE) hysteresis loop analysis

The PE loop measurements performed at room temperature have shown a slim hysteresis loop for all the ceramic compositions, contrary to the macroscopic cubic ($Pm\bar{3}m$) phase inferred from X-ray diffraction studies. With an increase in $Ca^{2+}(x)$ content, the remnant polarization shows an increasing trend till x = 0.15, and then it suddenly drops for x = 0.20 (see Fig. 3.6). Previous studies performed on similar Ca^{2+} doped $BaTiO_3$ system, *i.e.*, (Ba,Ca)TiO_3 have shown that the ferroelectric behaviour is governed by the cooperative effect of A(Ca^{2+}) and B(Ti^{4+}) site off-centered atom similar to $PbTiO_3$ [7, 49]. In $PbTiO_3$, the Pb-O bond exhibits a covalent nature, and the off-centered Pb^{2+} cation increases the hybridization between B(Ti^{4+}) site and oxygen atoms and reduces the short-range repulsion, which leads to enhancement in the ferroelectric displacement of B(Ti^{4+}) site cation [16, 49]. However, in (Ba,Ca)TiO_3, the nature of Ca-O bonding is ionic, and Ca^{2+} cation has an

off-centering tendency due to its smaller ionic radii. The off-centered Ca^{2+} cation at the 'A' site works cooperatively with the off-centered B(Ti^{4+}) site cations compatible with the tetragonal symmetry of lead-titanate [7, 49]. Recently, the observations made by Singh *et al.* on a similar system (Ba,Sr)(Sn,Ti)O_3 have also suggested a cooperative nature of the off-centered cations corresponding to 'A' and 'B' sites in the macroscopic cubic ($Pm\bar{3}m$) matrix [14]. Thus, despite having a cubic ($Pm\bar{3}m$) phase of BCSZTx ceramics, Ca^{2+} cation may have an off-centering tendency due to its smaller ionic radii [7], in addition to the locally off-centered Ti^{4+} cations as observed in $BaTiO_3$ [103, 107]. This leads to additional dipoles, which is clearly evident from the composition (x) dependent polarization of BCSZTx ceramics (see Fig. 3.6). On combining this analysis (dipoles generated due to the off-centered atoms corresponding to 'A' and 'B' sites of the macroscopic cubic matrix) with dielectric studies, which have shown an increase in relaxor behaviour with increasing Ca^{2+}(x) content, one can conclude that interaction between the dipoles, leading to the formation of polar nano-regions (intrapolar cluster, hereafter described as the phase I) is increasing, and also the increase in polarization suggests that the interaction between these PNRs (interpolar cluster, hereafter described as phase II) is also increasing with an increase in Ca^{2+}(x) content. Thus the increase in polarization (see Fig. 3.6) and the increase in dielectric relaxation behaviour (see Fig. 3.3) suggests that the strength of the above-mentioned phases, *viz.,* phase I and phase II increases with an increase in Ca^{2+}(x) content in BCSZTx matrix. The enhancement in the strength of phase I and phase II via increase of calcium content is analogous to the temperature-dependent behaviour of relaxor ferroelectrics, where the increase in the size and number of PNRs is observed with the decrease in temperature [10]. The observed anomaly in the remnant polarization and coercive field for $x = 0.20$ is related to the appearance of a new paraelectric phase which is $CaTiO_3$ like having an orthorhombic structure with a centrosymmetric *Pbnm* space group (shown by an arrow mark in Fig. 3.2(e)).

3.3.4 Raman spectroscopic studies

In order to ascertain the presence of short-range ordering responsible for relaxor ferroelectric behaviour and slim hysteresis loop, we have performed the Raman spectroscopic measurements for all the BCSZT*x* ceramic compositions. In a recent study on (Ba,Ca)TiO_3, an off-centering tendency of Ca^{2+} and Ti^{4+} cations having a cooperative nature has been observed by Fu *et al.* [7]. In addition, another study performed by us clearly demonstrates the presence of local off-centered displacements corresponding to the 'A' and 'B' site cations on a similar system, *viz.,* (Ba,Sr)(Sn,Ti)O_3 having long-range cubic phase with $Pm\bar{3}m$ space group [14]. In this study [14], the local off-centering of the atoms was probed by the Rietveld refinements by providing the local shifts in atomic coordinates along different directions despite of cubic phase where the atomic coordinates are fixed in the refinements. After carrying out the refinements by allowing the atoms to be locally displaced along various directions, we have observed the best agreement factors (R_{wp}) when the atoms corresponding to 'A' and 'B' sites were allowed to be displaced along <100> and <111> directions, respectively (see Fig. 3.7). Furthermore, the simultaneous displacement of the 'A' and 'B' site cations led to the best fit with the lowest value of the R_{wp} parameter, dictating a cooperative local off-centering of the cations corresponding to 'A' and 'B' sites [14]. Moreover, the Raman spectroscopic measurements performed on such systems like as Ba(Zr,Ti)O_3 and Ba(Sn,Ti)O_3 have shown rhombohedral-like polar clusters within the cubic phase field [187, 189, 238]. In the rhombohedral phase, the modes corresponding to T_{1u} phonons belonging to the $Pm\bar{3}m$ space group split into A_1 and E modes, while those corresponding to T_{2u} phonons split into A_2 and E modes. Out of these, A_1 and E modes exhibit Raman active nature, and the A_2 mode has no Raman activity. These optical modes further split into transverse (TO) and longitudinal (LO) modes due to electrostatic interactions [238, 239, 240]. The measured Raman spectra of BCSZT*x* ceramics consist of total seven peaks around 61.5, 106.4, 185.2, 258.2, 293.9, 512.8, and 717.5 cm^{-1} that cor-

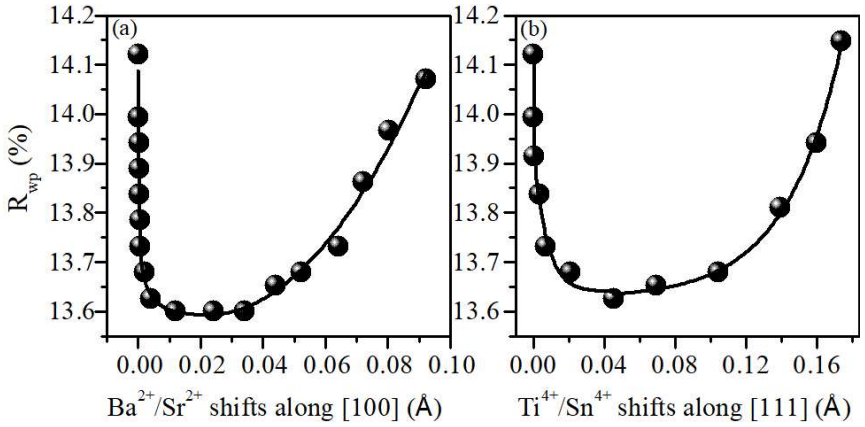

Fig. 3.7 Variation of agreement factor (R_{wp}) after providing local displacements to the cations corresponding to 'A' and 'B' sites along [100] and [111] directions, respectively [14].

responds to different Raman active modes. In addition to these peaks, a dip has also been observed around 123.3 cm^{-1}. The peak around 61.5 cm^{-1} is related to the A-O vibrations and corresponds to the disorder generated by 'A' site cations [241]. The peak around 106.4 cm^{-1} corresponds to E[TO1] mode, which is related to the presence of Sn and Zr-based clusters having a local rhombohedral structure [189, 227, 238, 242]. This peak appears if the size of the Sn and Zr rich domains encompasses approximately tens of unit cells so that a definite Raman spectrum can be generated by the phonons [189, 227]. The peaks present around 185.2 cm^{-1} and 258.2 cm^{-1} correspond to the modes A_1[TO1] and A_1[TO2], respectively [227]. These peaks are related to the B-O vibrations [243]. The A_1[TO1] mode comprises the displacements of 'B' site and oxygen ions relative to 'A' site cations, and A_1[TO2] mode comprises the displacements of 'B' site cation with respect to both the oxygen and 'A' site cations [239, 243, 244]. While the peak corresponding to the mode E[TO2], around 293.9 cm^{-1}, results due to the asymmetry in [BO_6] octahedra [245]. The appearance of this peak is due to the presence of different ionic radii cations $Sn^{4+}/Zr^{4+}/Ti^{4+}$ at the 'B' site, which leads to the distortion in the octahedra [246]. The above-mentioned peaks corresponding to the wavenumber 185.2 cm^{-1}, 258.2 cm^{-1}, and 293.9 cm^{-1} have

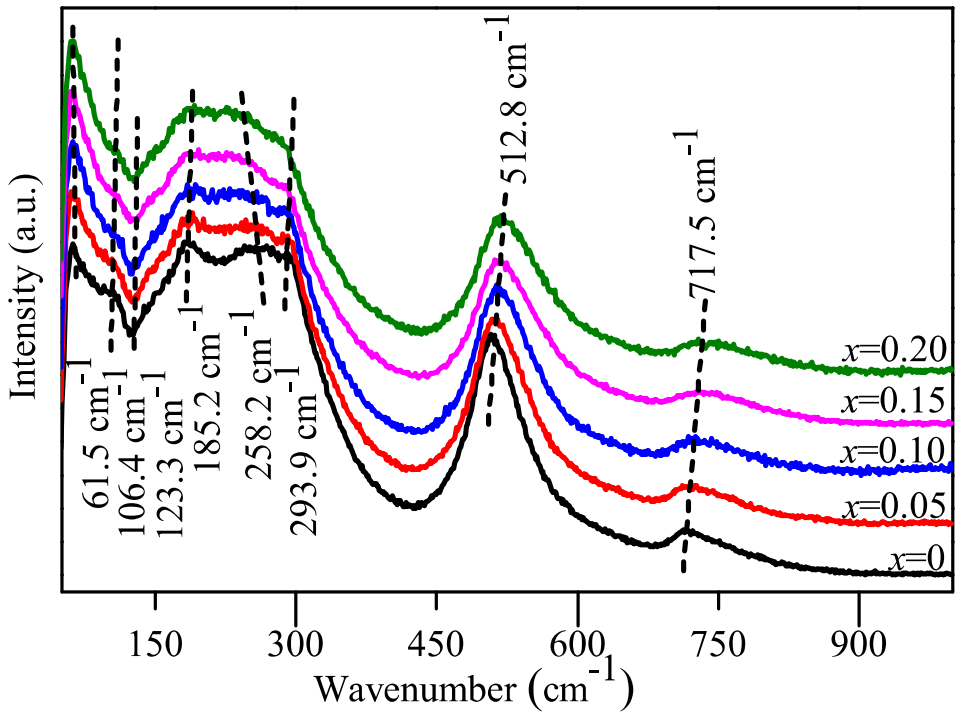

Fig. 3.8 Room temperature Raman spectra of BCSZTx ($0 \leq x \leq 0.20$) ceramics.

shown a broadened nature. The broadened nature of the peaks corresponds to the presence of disorder in the system [244, 247]. Further, the dip around 123.3 cm^{-1} is attributed to an interference effect of A_1[TO] phonon modes, *viz.*, A_1[TO1] and A_1[TO2]. This dip arises due to the presence of different ionic radii cations corresponding to B(Sn^{4+}/Zr^{4+}/Ti^{4+}) site [189]. Furthermore, the peak around 512.8 cm^{-1} corresponding to A_1[TO3] mode is due to O-Ti-O symmetric stretching vibrations, and it is related to the concentration of polar [TiO_6] octahedra in the cubic matrix [248]. The fitting of the Raman spectra (see Fig. 3.9) has shown that the width of this peak is approximately increasing with the increase in $Ca^{2+}(x)$ content (see Fig. 3.10), indicating an increase in structural disorder in the ceramics. This peak has shown a shift towards the higher wavenumber (see Fig. 3.10), which is ascribed as an increase in the force constant with the increase in the concentration of $Ca^{2+}(x)$ content at 'A' site [160]. The presence of different TO excitations in the macroscopically cubic structure reveals the presence of ferroelectric-like distortions [249].

Earlier, Margaritescu *et al.* reported that almost all the LO modes disappear in the absence of long-range ferroelectric ordering, but one can see the presence of A_1[LO3]/E[LO3] mode around 717.5 cm^{-1} for all compositions , which indicates the presence of sufficient

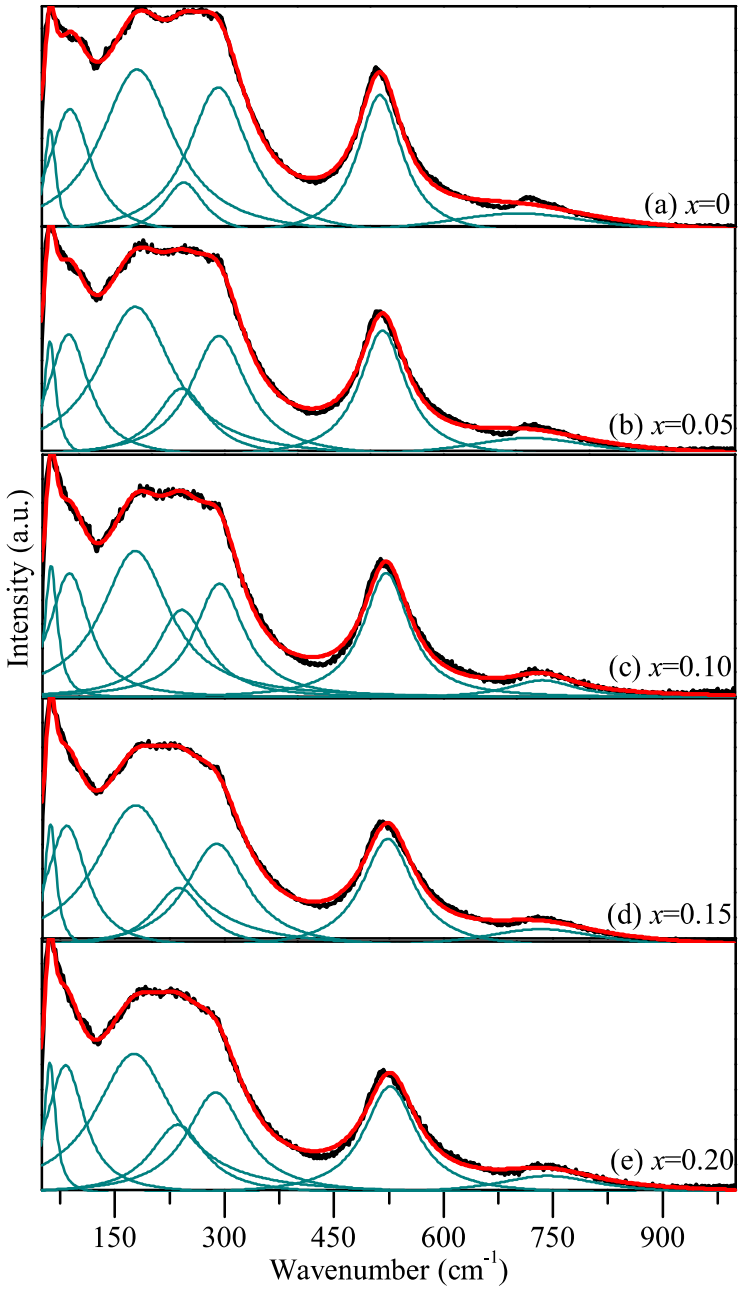

Fig. 3.9 The peak fitting for the Raman spectra of BCSZTx ($0 \leq x \leq 0.20$) ceramics.

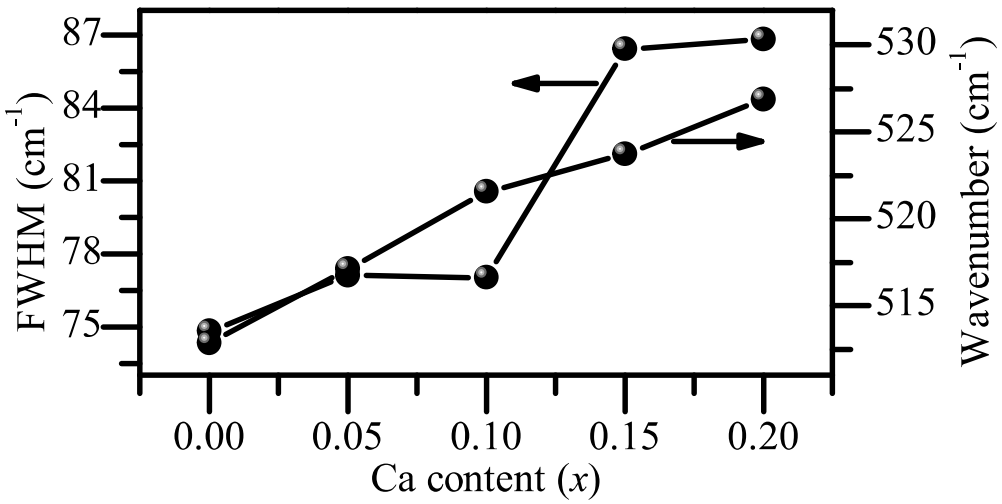

Fig. 3.10 The variation in peak width and position for 512.8 cm^{-1} mode as a function of Ca content.

electrostatic field even in the macroscopically cubic phase caused by the local disorder corresponding to 'A' and 'B' site cations [249]. In the $Ba(Sn,Ti)O_3$ system, Veselinovic *et al.* associated these A_1[LO3]/E[LO3] modes with the presence of distorted polar [TiO_6] clusters in the macroscopically cubic phase [165]. Fig. 3.8 has shown a broadened nature of this peak. This broadening is attributed to the presence of disorder in [TiO_6] octahedra. Hence we see that the substitution of Ca^{2+} at the 'A' site increases the distortion in the octahedra and promotes the 'B' site off-centering, resulting in the nucleation and growth of the PNRs [160, 226]. The above-mentioned long and short-range ordering is consistent with the dielectric studies, which show an increase in the relaxor behaviour with the increase in $Ca^{2+}(x)$ content. Thus the observed increase in relaxor behaviour and ferroelectric polarization, combined with Raman spectroscopic studies clearly suggest that in BCSZTx ceramics, the strength of the aforementioned exotic condensed phases present in the basic cubic ($Pm\bar{3}m$) matrix, *viz.,* intrapolar cluster (phase I), which generates polar nano-regions, and the interpolar cluster (phase II) that comprises the interaction between the polar nano-regions, increases with an increase in $Ca^{2+}(x)$ content. Moreover,

the host material of the explored ceramic system, *i.e.,* $Ba(Sn_{0.11}Ti_{0.89})O_3$, is well known for its high dielectric and piezoelectric properties due to the existence of a quadruple point slightly above room temperature and exhibits a transformation from macroscopic (global) rhombohedral to a macroscopic (global) cubic phase on increasing temperature [8]. However, the temperature-dependent dielectric studies of BCSZTx ceramics have shown a diffuse peak (see Fig. 3.3), and the Raman spectroscopic analysis has shown the presence of E[TO1] mode around 106.4 cm^{-1} (indicating the presence of local polar clusters with rhombohedral symmetry [189, 238]) for all the compositions (see Fig. 3.8), suggesting that the phase transition from macroscopic rhombohedral to macroscopic cubic symmetry, in BCSZTx ceramics is mediated via microscopically (short-range) ordered rhombohedral like polar clusters.

3.4 Conclusion

In conclusion, the work demonstrates the significant role of $Ca^{2+}(x)$ dopant in developing an 'A' site tunable eco-friendly smart material BCSZTx, synthesized at low temperatures, which is cost-effective and important from scientific as well as technological point of view. BCSZTx ceramics show an average cubic ($Pm\bar{3}m$) structure with a slim hysteresis loop and a relaxor ferroelectric behaviour for all the compositions. The observed polarization and the dielectric relaxation have shown an enhancement with the increase in $Ca^{2+}(x)$ content, owing to the off-centering of Ca^{2+} cations due to its smaller ionic radii and increased strength of the dipoles corresponding to the 'B' site cations. The role of Ca^{2+} dopant at the 'A' site in tuning the size and interaction of PNRs is analogous to the effect of temperature in relaxors. Moreover, the Raman spectroscopic studies combined with dielectric analysis have revealed that the macroscopic rhombohedral to the macroscopic cubic phase transition is mediated via microscopic rhombohedral-like polar clusters in BCSZTx ceramics. Owing to the diffuse nature of phase transition with a high value of dielectric constant and a

slim hysteresis loop, BCSZT*x* ceramics can act as a potential candidate for energy storage capacitors.

In the next chapter, we have analysed the temperature-dependent crystallographic structural evolution corresponding to composition Ca(x) = 0.15.